Hindawi Publishing Corporation
Shock and Vibration
Volume 2014, Article ID 741765, 15 pages
http://dx.doi.org/10.1155/2014/741765

Research Article

Adaptive Model Predictive Vibration Control of a Cantilever Beam with Real-Time Parameter Estimation

Gergely Takács, Tomáš Polóni, and Boris Rohaľ-Ilkiv

Slovak University of Technology in Bratislava, Faculty of Mechanical Engineering, Institute of Automation, Measurement and Applied Informatics, Nám Slobody 17, 812 31 Bratislava 1, Slovakia

Correspondence should be addressed to Gergely Takács; gergely.takacs@stuba.sk

Received 14 August 2013; Revised 14 March 2014; Accepted 15 March 2014; Published 7 May 2014

Academic Editor: Hongyi Li

This paper presents an adaptive-predictive vibration control system using extended Kalman filtering for the joint estimation of system states and model parameters. A fixed-free cantilever beam equipped with piezoceramic actuators serves as a test platform to validate the proposed control strategy. Deflection readings taken at the end of the beam have been used to reconstruct the position and velocity information for a second-order state-space model. In addition to the states, the dynamic system has been augmented by the unknown model parameters: stiffness, damping constant, and a voltage/force conversion constant, characterizing the actuating effect of the piezoceramic transducers. The states and parameters of this augmented system have been estimated in real time, using the hybrid extended Kalman filter. The estimated model parameters have been applied to define the continuous state-space model of the vibrating system, which in turn is discretized for the predictive controller. The model predictive control algorithm generates state predictions and dual-mode quadratic cost prediction matrices based on the updated discrete state-space models. The resulting cost function is then minimized using quadratic programming to find the sequence of optimal but constrained control inputs. The proposed active vibration control system is implemented and evaluated experimentally to investigate the viability of the control method.

1. Introduction

Undesirable mechanical and structural vibrations may often cause discomfort in humans and in certain engineering applications can even lead to catastrophic failure or other extreme consequences. Passive vibration attenuation approaches are popular in engineering practice, but the required structural changes tend to get troublesome with low frequency vibrations [1, 2]. With the advent of new actuator and sensor types and the availability of cheap computing technology, active vibration control (AVC) has become an important tool in managing excessive vibration levels [3, 4].

When designing the algorithm support for AVC systems, a frequent assumption is that the controlled structure maintains its dynamic properties throughout the control procedure. This assumption enables the straightforward tuning of some controllers used in vibration attenuation like positive position feedback (PPF) [2, 4], while, in model-based algorithms such as linear quadratic (LQ) [3, 5] or model predictive control [6–8] (MPC), it allows the use of a relatively precise nominal model. However, not every AVC application fits this convenient premise. A time-varying system behavior may simply detune the controller causing it to operate with suboptimal performance, but it may also affect the stability of the closed-loop control system. Also, one of the most important properties of self-reliant structural control systems is adaptivity, implying a degree of in situ intelligence [9].

One of the possible ways to handle model and parameter changes is robust controller design. The basis of the design approach is the a priori analysis of system behavior given a compact set of uncertain parameters. Within this predefined bounded set, the controller remains stable and fulfills certain tradeoff performance criteria; nevertheless, the best performance is usually achieved only with the nominal model. Robust versions of numerous well-known control methods have been considered for the control of vibrating mechanical structures, including robust pole-placement [10], robust H_∞ [11], robust LQ [12], and robust min–max LQ [1]. Nonetheless,

a real adaptive vibration control system offering a degree of self-reliance requires advanced control looking beyond the boundaries of mere robustness [9].

In addition to robust controller design practices, the problem of variable structural properties is often addressed by introducing a level of adaptivity into the control loop. Adaptivity enables the vibration control system to function under varying load conditions, partial actuator failure, or performance degradation, a limited change in geometric configuration or varying physical parameters. Modeling uncertainties—and to a degree nonlinearities—can be also compensated by adaptivity [13]. Thus, the advantage of adaptive algorithms in general is their superior performance, although they tend to be computationally more expensive than robust implementations. An excellent overview of adaptive structural control with a focus on self-reliance is given by Hyland and Davis in [9].

Possibly one of the best known and most widely used adaptive methods applied for AVC and especially active noise control (ANC) is the least mean square (LMS) feedforward control [14–16], where the changes in system dynamics are translated into the coefficient variations in the adaptive finite impulse response filter (FIR). A frequent choice of adaptive AVC encountered in literature is model reference adaptive control (MRAC) [13], which does not require the use of explicitly defined system parameters [17]. Other adaptive vibration control schemes proposed in the past include sliding mode control [18, 19], neural networks [20, 21], or an adaptive control scheme featuring a high-gain observer for compensating model errors, which was introduced for vibrating microcantilevers by Zhang et al. [22]. Suitable online identification methods for adaptive AVC include the subspace identification or autoregressive moving average (ARMAX) models, adaptive feedforward control, while variants of the extended Kalman filter (EKF) have been used for real-time modal parameter diagnostics applications [23].

In order to formulate an adaptive vibration controller, instead of identifying the coefficients in FIR filters or using the models without explicit parameterization, we apply the augmented continuous-discrete extended Kalman filter [24–26] to estimate the dynamic states as physically interpretable parameters of a vibrating mechanical system, such as the stiffness and damping coefficient. The extended Kalman filter is possibly the most widely used algorithm for the estimation of states and parameters of nonlinear dynamic systems [24]; here, it performs the online parameter identification for adaptive-predictive vibration control. The use of EKF or its alternatives to identify the parameters of vibrating systems is also common; however, most of these methods involve offline parameter estimation from measured data or online diagnostics and do not use EKF in real-time to supplement model data to model-based control systems. Examples include disturbance force estimation on a free-free beam [27], health monitoring of base-isolated structures under seismic loads [28], and stiffness and damping coefficient estimation in hydromount systems for reducing vibrations in automotive applications [29]. Recently, Szabat and Orlowska-Kowalska used the extended Kalman filter to adaptively control torsional vibration in a two-mass rotating drive system [30, 31]. The EKF was previously used as a benchmark algorithm for the open-loop state and parameter estimation of the free vibrations of the cantilever beam considered in this work, contrasting the results to moving horizon observer (MHO) in an offline simulation [32].

In this work, the parameters estimated by the EKF are used to update the continuous model, which is in turn discretized, to create the state predictions for an input constrained infinite horizon dual-mode MPC algorithm [33, 34]. Regarded by many as one of the most important developments in control engineering [35], the key advantage of using a model-based predictive algorithm in any system is that it can take the effect of future state, input, or output constraints into account when computing the control move [36]. Constraints are essential in every application field, but piezoceramics often used in vibration control are particularly prone to failure and performance degradation by depolarization, which may occur if voltage limits are continually exceeded [8, 37]. The explicit constraint handling feature offered by the MPC method is unique and valuable property amongst the available control algorithms [34]. In addition to this hallmark feature, the performance of a well-designed and tuned MPC algorithm may surpass other traditional control strategies used in vibration control. This is due to the fact that model predictive control is an optimal control method. A significant drawback of using advanced optimization-based control methods such as the MPC is the computational cost of solving the problem online [6, 37].

The combination of EKF and MPC resulting in the proposed adaptive EKF-MPC vibration control scheme is applied to a clamped aluminum cantilever beam which is equipped with piezoceramic transducers and its deformation is measured at the free end using a laser triangulation system (Figure 1). Let us assume that the dynamics of this beam can be modeled using a second-order differential equation describing the motion of the point-mass-damper system. This assumption holds true, if the first resonance of the structure dominates the dynamic response, which is the case for a class of real-life structures [8, 38]. It is necessary to use such a simple dynamic model in order to ensure the real-time feasibility of the computation intensive quadratic programming solver required for constrained MPC. Furthermore, let us assume that the force contribution from the actuators can be modeled by the input voltage multiplied by a scalar conversion constant and that the beam is excited by an external shock-like disturbance force.

The disturbance force is a series of impacts delivered to the beam, emulating the release test similar to transient vibration typical for aerospace structures [39]. The aim of the adaptive EKF-MPC vibration control algorithm then is to attempt to keep the beam position near its equilibrium using constrained inputs and despite the external disturbances, while continually adapting to possible changes in the dynamic behavior by observing the unknown system parameters in addition to the system states. The control system will shorten the overall settling time of the structure and concurrently adapt the algorithm properties to parameter changes.

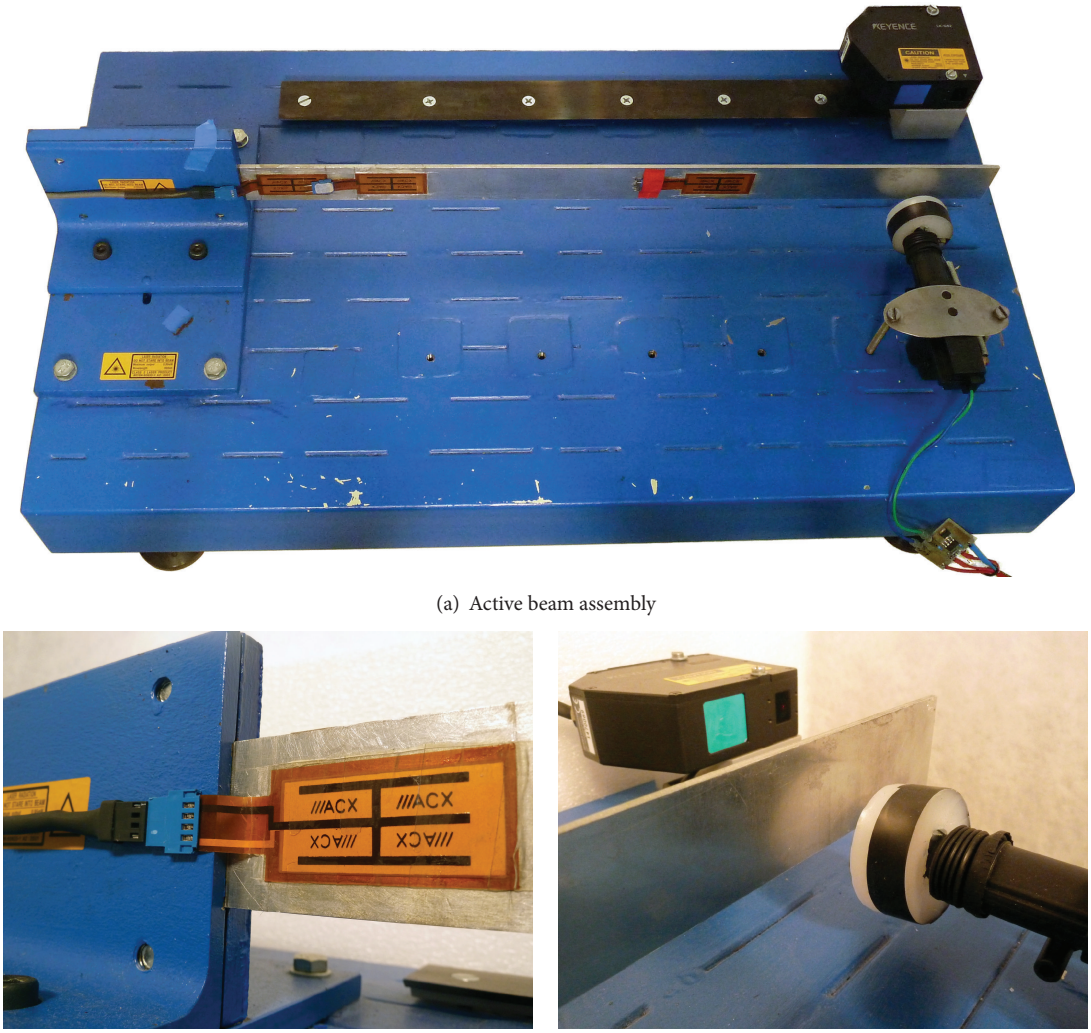

(a) Active beam assembly

(b) Piezoceramic actuators

(c) Laser feedback and stinger

Figure 1: Clamped cantilever with active vibration control.

The vibration control algorithm proposed here unifies the advantages of the adaptivity enabled by the online extended Kalman filter and constrained model predictive control. The EKF-MPC method offers greater damping performance in the face of time-varying physical parameters and model uncertainties, while at the same time ensuring the fulfillment of process constraints in order to increase the safety and reliability of modern AVC systems. The advantages introduced above come at a price, which is mainly the increase in complexity and computational load.

After the formerly presented introductory section, the theoretical methodology of the work is discussed in Section 2. First, the modeling of the dynamics of the vibrating cantilever including the parameter augmentation is presented; then, we review the formulation of the extended Kalman filter for the given problem. The discretization procedure of the continuous system model and the constrained model predictive algorithm is followed by an overall summary of the proposed EKF-MPC vibration control algorithm. Section 3 presents the experimental hardware in more detail along with the common assumptions and utilized settings, while the different experimental scenarios are also introduced in this section. We report the results of the experiments and discuss their meaning in Section 4 and, finally, the paper is concluded in Section 5.

2. Methodology

2.1. System Dynamics Augmented by Unknown Parameters. Let us assume that the vibration dynamics of the fixed-free cantilever beam can be approximated by a second-order differential equation describing the motion of a spring-mass-damper with an external force input [3, 4] and an unknown external disturbance

$$m\ddot{q}(t) + b\dot{q}(t) + kq(t) = cu(t) + F_e(t), \tag{1}$$

where m (kg) is the equivalent mass of the beam and the actuators, b (Ns/m) is the equivalent viscous damping coefficient, and k (N/m) is the equivalent stiffness; let c (N/V) represent the scalar coefficient transforming input voltage to

force $F(t) = cu(t)$ (N) and let $F_e(t)$ (N) be the disturbance [40]. The input to this system is the voltage supplied to the actuators $u(t)$ (V) and the single measured output is the position of the beam $q(t)$ (m).

Such a second-order differential equation representing a 1 DOF vibrating system only takes the first resonant frequency into account; however, from the viewpoint of the control system, this is not an issue, since the first resonance dominates the response. Single degree of freedom models are routinely used in literature to identify the physical parameters of vibrating structures using the EKF and other statistical estimation methods [32, 41, 42].

If we choose the position and velocity as state variables $(x_1(t) = q(t), x_2(t) = \dot{q}(t))$, it is possible to express this equation in a continuous, linear, state-space form

$$\dot{\mathbf{x}}(t) = \mathbf{\Phi}\mathbf{x}(t) + \mathbf{\Gamma}u(t) + \mathbf{\Theta}F_e(t), \tag{2}$$

$$y(t) = \mathbf{C}\mathbf{x}(t). \tag{3}$$

Matrix $\mathbf{\Phi} \in \mathbb{R}^{2\times 2}$ is the dynamics matrix, $\mathbf{\Gamma} \in \mathbb{R}^{2\times 1}$ is the input matrix, and $\mathbf{\Theta} \in \mathbb{R}^{2\times 1}$ is the unknown force transition matrix, which for the assumed model take the following form [40, 43]:

$$\mathbf{\Phi} = \begin{bmatrix} 0 & 1 \\ -\frac{k}{m} & -\frac{b}{m} \end{bmatrix} \qquad \mathbf{\Gamma} = \begin{bmatrix} 0 \\ \frac{c}{m} \end{bmatrix} \qquad \mathbf{\Theta} = \begin{bmatrix} 0 \\ \frac{1}{m} \end{bmatrix}. \tag{4}$$

Furthermore, $\mathbf{C} = [1\ \ 0]$ outputs the position $y(t) = q(t)$ (m), measured at a single point at the beam tip, while direct input feedthrough is omitted in this case. Assuming that the equivalent mass m is known and constant but other parameters may vary with time, the system dynamics noted as $\mathbf{\Phi}(t)$ and $\mathbf{\Gamma}(t)$ are time variable and are continually updated in the EKF-MPC algorithm.

The continuous state $\mathbf{x}(t)$ describing only the system dynamics as defined in (2) can be augmented by the vector of unknown parameters $\mathbf{p}(t)$. In this case,

$$\mathbf{p}(t) = \begin{bmatrix} k(t) & b(t) & c(t) & F_e(t) \end{bmatrix}^T, \tag{5}$$

where $\mathbf{p}(t)$ is expressing the unknown and potentially changing damping, stiffness, force conversion parameter, and the external disturbance. The new augmented state becomes

$$\mathbf{x}_a(t) = \begin{bmatrix} \mathbf{x}(t) & \mathbf{p}(t) \end{bmatrix}^T. \tag{6}$$

The system dynamics, which is augmented by the unknown parameters, can be expressed as

$$\begin{aligned} \dot{\mathbf{x}}(t) &= \widetilde{f}_c(\mathbf{x}(t), \mathbf{p}(t), u(t)) + w_s(t), \\ \dot{\mathbf{p}}(t) &= w_p(t), \end{aligned} \tag{7}$$

where $w_s(t)$ is the system process noise and $w_p(t)$ is the parameter process noise. Equation (7) can be combined to get the augmented dynamics

$$\dot{\mathbf{x}}_a(t) = f_c(\mathbf{x}_a(t), u(t)) + w(t), \tag{8}$$

$$\begin{aligned} y(t) &= h(\mathbf{x}_a(t), u(t)) + v(t) \\ &= \begin{bmatrix} 1 & 0 & 0 & 0 & 0 & 0 \end{bmatrix} \mathbf{x}_a(t) + v(t), \end{aligned} \tag{9}$$

where the function f_c represents the continuous augmented dynamics, h_c is the continuous measurement function, and $w(t) = [w_s(t)\ \ w_p(t)]^T$ expresses system and parameter process noise. The process noise and measurement noise have the properties of white noise; in other words, they have a sequentially uncorrelated Gaussian distribution with a zero mean:

$$\begin{aligned} w(t) &\sim N(0, \mathbf{Q}_{ft}), \\ v(t) &\sim N(0, \mathbf{R}_f), \end{aligned} \tag{10}$$

where $\mathbf{Q}_{ft}$ is a process noise covariance matrix and $\mathbf{R}_f$ is a measurement noise covariance matrix.

Note that, by augmenting the dynamics of the mass-spring-damper system by the parameters in (8) and (9), we essentially turn the otherwise linear state-space model into a nonlinear formulation, since the parameters will be used in multiplicative operations inside the model [24, 25].

Even though the real system dynamics is continuous in nature, in practice the output can be only observed at discrete sampling times $t = kT, k = 1, 2, 3, \ldots$, where T is the sampling interval. Therefore, we will consider a numerically simulated nonlinear system [24] described and propagated by

$$\begin{aligned} \mathbf{x}_{a(k+1)} &= f(\mathbf{x}_{a(k)}, u_{(k)}) + w_{(k)}, \\ y_{(k)} &= h(\mathbf{x}_{a(k)}, u_{(k)}) + v_{(k)} \\ &= \begin{bmatrix} 1 & 0 & 0 & 0 & 0 & 0 \end{bmatrix} \mathbf{x}_{a(k)} + v_{(k)}. \end{aligned} \tag{11}$$

2.2. Hybrid Extended Kalman Filter. The EKF algorithm is commonly used to estimate the parameters of nonlinear dynamic systems and the variant summarized here is known in literature as the continuous-discrete or hybrid EKF [24]. The EKF [24, 25] is initialized with the initial estimate of the augmented state

$$\hat{\mathbf{x}}_{a0}^{+} = E[\mathbf{x}_{a0}] \tag{12}$$

and the covariance matrix of the initial state error estimate

$$\mathbf{P}_0^{+} = E\left[(\mathbf{x}_{a0} - \hat{\mathbf{x}}_{a0}^{+})(\mathbf{x}_{a0} - \hat{\mathbf{x}}_{a0}^{+})^T\right]. \tag{13}$$

To obtain the a priori state estimate (denoted by the $^-$ subscript) in the continuous part of the filter, the state estimate of the augmented dynamic system (8) is simulatively propagated from time $t = (k-1)$ one step ahead to the next time instant $t = (k)$

$$\hat{\mathbf{x}}_{a(k)}^{-} = f\left(\hat{\mathbf{x}}_{a(k-1)}^{+}, u_{(k)}\right), \tag{14}$$

using the system dynamics of the mass-spring-damper augmented by the change in parameters $\mathbf{p}(t) = [k(t)\ \ b(t)\ \ c(t)\ \ F_e(t)]^T$

$$\dot{q}(t) = \dot{x}_1(t) = x_2(t)$$

$$\ddot{q}(t) = \dot{x}_2(t) = -\frac{1}{m}x_3(t)\,x_1(t) - \frac{1}{m}x_4(t)\,x_2(t)$$

$$+ \frac{1}{m}x_5(t)\,u(t) + \frac{1}{m}x_6(t)$$

$$\begin{aligned}\dot{k}(t) &= \dot{x}_3(t) = 0\\ \dot{b}(t) &= \dot{x}_4(t) = 0\\ \dot{c}(t) &= \dot{x}_5(t) = 0\\ \dot{F}_e(t) &= \dot{x}_6(t) = 0.\end{aligned} \tag{15}$$

The time update of the a priori covariance matrix estimate [24, 25] is given by the equation

$$\dot{\mathbf{P}}(t) = \mathbf{Z}\left(\hat{\mathbf{x}}_a(t)\right)\mathbf{P}(t) + \mathbf{P}(t)\,\mathbf{Z}^T\left(\hat{\mathbf{x}}_a(t)\right) + \mathbf{Q}_{ft}, \tag{16}$$

where the Jacobian of the state equation (15) is expressed by

$$\mathbf{Z}\left(\hat{\mathbf{x}}_a\right) = \left.\frac{\partial f_c(\mathbf{x}_a)}{\partial \mathbf{x}_a}\right|_{\mathbf{x}_a=\hat{\mathbf{x}}_a} = \begin{bmatrix} 0 & 1 & 0 & 0 & 0 & 0\\ -\frac{1}{m}x_3(t) & -\frac{1}{m}x_4(t) & -\frac{1}{m}x_1(t) & -\frac{1}{m}x_2(t) & \frac{1}{m}u(t) & \frac{1}{m}\\ 0 & 0 & 0 & 0 & 0 & 0\\ 0 & 0 & 0 & 0 & 0 & 0\\ 0 & 0 & 0 & 0 & 0 & 0\\ 0 & 0 & 0 & 0 & 0 & 0 \end{bmatrix}_{\mathbf{x}_a=\hat{\mathbf{x}}_a}. \tag{17}$$

Concluding the continuous part of the hybrid EKF, the covariance matrix estimate is obtained by simulative propagation of (16) from time $t = (k-1)$ to the sample at $t = (k)$

$$\mathbf{P}^-_{(k)} = g\left(\mathbf{P}^+_{(k-1)}, \mathbf{Z}\left(\hat{\mathbf{x}}^+_{a(k-1)}\right)\right). \tag{18}$$

The Kalman gain matrix at sample (k) is

$$\mathbf{K}_{f(k)} = \mathbf{P}^-_{(k)}\mathbf{L}^T\left[\mathbf{L}\mathbf{P}^-_{(k)}\mathbf{L}^T + \mathbf{M}\mathbf{R}_f\mathbf{M}^T\right]^{-1}. \tag{19}$$

The augmented state estimate is updated to obtain the a posteriori estimate (denoted by the $^+$ subscript) along with the a posteriori update of the error covariance matrix

$$\hat{\mathbf{x}}^+_{a(k)} = \hat{\mathbf{x}}^-_{a(k)} + \mathbf{K}_{f(k)}\left[y_{(k)} - h\left(\hat{\mathbf{x}}^-_{a(k)}, u_{(k)}\right)\right], \tag{20}$$

$$\mathbf{P}^+_{(k)} = \left[\mathbf{I} - \mathbf{K}_{f(k)}\mathbf{L}\right]\mathbf{P}^-_{(k)}\left[\mathbf{I} - \mathbf{K}_{f(k)}\mathbf{L}\right]^T + \mathbf{K}_{f(k)}\mathbf{M}\mathbf{R}_f\mathbf{M}^T\mathbf{K}^T_{f(k)}, \tag{21}$$

using the Jacobians of the measurement equation $h(\mathbf{x}_{a(t)})$ with respect to $\mathbf{x}_{a(t)}$ and $\mathbf{v}_{a(t)}$

$$\begin{aligned}\mathbf{L}_{(k)} &= \left.\frac{\partial h(\mathbf{x}_{a(t)})}{\partial \mathbf{x}_{a(t)}}\right|_{\mathbf{x}_{a(t)}=\hat{\mathbf{x}}^-_{a(t)}} = \begin{bmatrix}1 & 0 & 0 & 0 & 0 & 0\end{bmatrix}\\ \mathbf{M}_{(k)} &= \left.\frac{\partial h(\mathbf{x}_{a(t)})}{\partial \mathbf{v}_{a(t)}}\right|_{\mathbf{x}_{a(t)}=\hat{\mathbf{x}}^-_{a(t)}} = 1.\end{aligned} \tag{22}$$

Both $\hat{\mathbf{x}}^+_{a(k)}$ and $\mathbf{P}^+_{(k)}$ are stored and used in the next step of the a priori computation.

2.3. Model Updates and Discretization. The continuous model in (2) defined by $\mathbf{\Phi}_{(k)}$ and $\mathbf{\Gamma}_{(k)}$ is updated at discrete times (k) based on the latest available estimates of the parameters $k_{(k)}$, $b_{(k)}$, and $c_{(k)}$ by the EKF introduced in the previous section. The linear time-invariant MPC formulation assumed in this work expects a discrete-time model given by

$$\mathbf{x}_{(k+1)} = \mathbf{A}_{(k)}\mathbf{x}_{(k)} + \mathbf{B}_{(k)}u_{(k)}, \tag{23}$$

$$y_{(k)} = \mathbf{C}\mathbf{x}_{(k)}. \tag{24}$$

Matrix $\mathbf{A}_{(k)} \in \mathbb{R}^{2\times 2}$ is the dynamics matrix, $\mathbf{B}_{(k)} \in \mathbb{R}^{2\times 1}$ is the input matrix, and $\mathbf{C} = [1\ \ 0]$ outputs the position $y_{(k)} = x_{1(k)} = q_{(k)}$ (m). Using a discrete sampling time T (s), the continuous-time state and input matrices $\mathbf{\Phi}_{(k)}$ and $\mathbf{\Gamma}_{(k)}$ are discretized [44] using

$$\mathbf{A}_{(k)} = \mathbf{I} + \mathbf{\Phi}_{(k)}T\mathbf{\Psi}_{(k)}, \tag{25}$$

$$\mathbf{B}_{(k)} = \mathbf{\Psi}_{(k)}T\mathbf{\Gamma}_{(k)}, \tag{26}$$

where the term $\mathbf{\Psi}_{(k)}$ is expressed by the infinite series

$$\mathbf{\Psi}_{(k)} = \mathbf{I} + \frac{\mathbf{\Phi}_{(k)}T}{2!} + \frac{\mathbf{\Phi}_{(k)}T}{3!} + \frac{\mathbf{\Phi}_{(k)}T}{4!} + \cdots, \tag{27}$$

which in practice can be approximated using successive iterations j of [44]

$$\mathbf{\Psi}_{(k)} \approx \mathbf{I} + \frac{\mathbf{\Phi}_{(k)}T}{2}\left(\mathbf{I} + \frac{\mathbf{\Phi}_{(k)}T}{3}\left(\cdots\frac{\mathbf{\Phi}_{(k)}T}{j-1}\left(\mathbf{I} + \frac{\mathbf{\Phi}_{(k)}T}{j}\right)\right)\cdots\right). \tag{28}$$

2.4. Model Predictive Control. The online MPC optimization problem involves minimizing the cost function subject to constraints on the voltage input. The particular MPC method considered here is known as the infinite horizon constrained dual-mode MPC algorithm [33, 34]. After choosing a horizon of n steps, we may predict the evolution of the future states—compactly denoted by $\vec{\mathbf{x}}_{(k)}$—based on the estimate of the current state $\mathbf{x}_{0(k)} = \hat{\mathbf{x}}^+_{0(k)}$ (excluding parameters $\mathbf{p}(k)$) and the sequence of future inputs $\vec{u}_{(k)}$, at time (k) by the recursive substitution of states using (23) [34]. We may express this in a compact notation by [33, 34]

$$\vec{\mathbf{x}}_{(k)} = \mathbf{M}_{(k)}\mathbf{x}_{0(k)} + \mathbf{N}_{(k)}\vec{\mathbf{u}}_{(k)}, \tag{29}$$

where matrices $\mathbf{M}_{(k)}$ and $\mathbf{N}_{(k)}$ for step (k) are [33]

$$\mathbf{M}_{(k)} = \begin{bmatrix} \mathbf{A}_{(k)}^{0} & \mathbf{A}_{(k)}^{1} & \dots & \mathbf{A}_{(k)}^{n-2} & \mathbf{A}_{(k)}^{n-1} & \mathbf{A}_{(k)}^{n} \end{bmatrix}^{T} \tag{30}$$

$$\mathbf{N}_{(k)} = \begin{bmatrix} \mathbf{0} & \mathbf{0} & \dots & \mathbf{0} & \mathbf{0} & \mathbf{0} \\ \mathbf{B}_{(k)} & \mathbf{0} & \dots & \mathbf{0} & \mathbf{0} & \mathbf{0} \\ \mathbf{A}_{(k)}\mathbf{B}_{(k)} & \mathbf{B}_{(k)} & \dots & \mathbf{0} & \mathbf{0} & \mathbf{0} \\ \vdots & \vdots & \ddots & \vdots & \vdots & \vdots \\ \mathbf{A}_{(k)}^{n-1}\mathbf{B}_{(k)} & \mathbf{A}_{(k)}^{n-2}\mathbf{B}_{(k)} & \dots & \mathbf{A}_{(k)}^{2}\mathbf{B}_{(k)} & \mathbf{A}_{(k)}\mathbf{B}_{(k)} & \mathbf{B}_{(k)} \end{bmatrix}. \tag{31}$$

Let us define the linear, quadratic cost function, expressing the contribution of future states $\vec{\mathbf{x}}_{(k)}$ and future inputs $\vec{\mathbf{u}}_{(k)}$ into the numerical control quality indicator $J(\text{-})$. This cost function uses the dual-mode paradigm, utilizing free inputs for the first n steps and a fixed feedback controller afterwards [45]:

$$J_{(k)} = \sum_{i=0}^{n-1} \left(\mathbf{x}_{(k+i)}^{T} \mathbf{Q} \mathbf{x}_{(k+i)} + u_{(k+i)}^{T} \mathbf{R} u_{(k+i)} \right) + \mathbf{x}_{(k+n)}^{T} \mathbf{P}_{f(k)} \mathbf{x}_{(k+n)}, \tag{32}$$

where $\mathbf{Q} = \mathbf{Q}^{T} \geq 0$ is the user determined penalization matrix for states and $\mathbf{R} = \mathbf{R}^{T} \geq 0$ is the penalization matrix for inputs. Furthermore, $\mathbf{P}_{f(k)}$ is the solution of the unconstrained, infinite horizon quadratic regulation problem [33, 34, 45] at sample (k). The recursive feasibility of constraints to provide stability guarantees [46, 47] is not implemented in this work, so that the feasibility of the real-time implementation is ensured given the relatively short sampling periods of the vibration control problem [8, 37].

Unlike in the case of MPC with a nominal model, here the terminal weight $\mathbf{P}_{f(k)}$ must be recomputed online as the solution of the discrete-time algebraic Riccati equation (DARE) [48]:

$$\begin{aligned} &\mathbf{A}_{(k)}^{T} \mathbf{P}_{f(k)} \mathbf{A}_{(k)} - \mathbf{P}_{f(k)} \\ &- \mathbf{A}_{(k)}^{T} \mathbf{P}_{f(k)} \mathbf{B}_{(k)} \left(\mathbf{R} + \mathbf{B}_{(k)}^{T} \mathbf{P}_{f(k)} \mathbf{B}_{(k)} \right)^{-1} \mathbf{B}_{(k)} \mathbf{P}_{f(k)} \mathbf{A}_{(k)} \\ &+ \mathbf{Q} = 0. \end{aligned} \tag{33}$$

For the numerical solution of this classical control problem, amongst others, iterative cost reduction algorithms [49], Schur methods [50], or eigenvalue decomposition methods [48, 51] may be applied, of which we consider the latter procedure based on the work of Pappas et al. [48]. Let us define $\mathbf{G}_{(k)}$ as

$$\mathbf{G}_{(k)} = \mathbf{B}_{(k)} \mathbf{R}^{-1} \mathbf{B}_{(k)}^{T}. \tag{34}$$

Consider the generalized eigenvalue problem as

$$\mathbf{Y}_{(k)} \mathbf{V}_{(k)} = \mathbf{U}_{(k)} \mathbf{X}_{(k)} \mathbf{V}_{(k)}, \tag{35}$$

where $\mathbf{U}_{(k)}$ is the diagonal matrix containing generalized eigenvalues and the full matrix $\mathbf{V}_{(k)}$ corresponding to the generalized principal vectors of (35). We define $\mathbf{X}_{(k)}$ and $\mathbf{Y}_{(k)}$ as

$$\mathbf{X}_{(k)} = \begin{bmatrix} \mathbf{I} & \mathbf{G}_{(k)} \\ \mathbf{0} & \mathbf{A}_{(k)}^{T} \end{bmatrix} \qquad \mathbf{Y}_{(k)} = \begin{bmatrix} \mathbf{A}_{(k)} & \mathbf{0} \\ -\mathbf{Q} & \mathbf{I} \end{bmatrix}. \tag{36}$$

After solving (35), the diagonal matrix $\mathbf{U}_{(k)}$ can be used to identify the indices of stable eigenvalues. The eigenvectors of $\mathbf{V}_{(k)}$ that are corresponding to the identified stable eigenvalues can be inserted in a matrix $\mathbf{W}_{(k)}$ used as the basis of the stable eigenspace, which is partitioned into two submatrices

$$\mathbf{W}_{(k)} = \begin{bmatrix} \mathbf{W}_{1(k)} \\ \mathbf{W}_{2(k)} \end{bmatrix}. \tag{37}$$

Finally, the solution of the discrete-time algebraic Riccati equation in (33) can be computed as [48]

$$\mathbf{P}_{f(k)} = \mathbf{W}_{2(k)} \mathbf{W}_{1(k)}^{-1}. \tag{38}$$

Since the adaptive MPC algorithm considered here does not implement a recursive constraint checking horizon needed to guarantee stability on an infinite horizon [46, 47], it does not explicitly need the LQ gain itself, only the solution of the DARE. Nevertheless, this work uses the unconstrained equivalent LQ gain as a certain diagnostic indicator of the algorithm behavior. The unconstrained equivalent LQ gain can be computed by evaluating

$$\mathbf{K}_{(k)} = \left(\mathbf{R} + \mathbf{B}_{(k)}^{T} \mathbf{P}_{f(k)} \mathbf{B}_{(k)} \right)^{-1} \mathbf{B}_{(k)}^{T} \mathbf{P}_{f(k)} \mathbf{A}_{(k)}. \tag{39}$$

The model predictive control algorithm is formulated based on the minimization of the dual-mode cost in (32). To find the solution of the MPC problem at a given sample, one must execute the minimization [33, 34]

$$\begin{aligned} \min_{\mathbf{u}_k} J\left(\mathbf{u}_k, \mathbf{x}_k\right) = &\sum_{i=0}^{n-1} \left(\mathbf{x}_{(k+i)}^{T} \mathbf{Q} \mathbf{x}_{(k+i)} + u_{(k+i)}^{T} \mathbf{R} u_{(k+i)} \right) \\ &+ \mathbf{x}_{(k+n)}^{T} \mathbf{P}_{f(k)} \mathbf{x}_{(k+n)}, \end{aligned} \tag{40}$$

subject to the following constraints:

$$\underline{u} \leq u_{(k+i)} \leq \overline{u}, \quad i = 0, 1, 2, \dots, n-1 \tag{41}$$

$$\mathbf{x}_{0(k)} = \mathbf{x}_{(k)} \tag{42}$$

$$\mathbf{x}_{(k+1+i)} = \mathbf{A}_{(k)} \mathbf{x}_{(k+i)} + \mathbf{B}_{(k)} u_{(k+i)}, \quad i \geq 0 \tag{43}$$

$$y_{(k+i)} = \mathbf{C} \mathbf{x}_{(k+i)}, \quad i \geq 0 \tag{44}$$

$$u_{(k+i)} = \mathbf{K}_{(k)} \mathbf{x}_{(k+i)}, \quad i \geq n, \tag{45}$$

where (41) expresses the predefined process constraints on the voltage levels, (42) is the observed dynamic state containing position and velocity estimates, (43) and (44) are the discrete linear state-space model updated by the parameters, and (45) is the constraint which is implicitly included in the terminal cost and, due to the receding horizon implementation, it is never realized.

In order to make this optimization procedure suitable for numerical solvers, the cost and the constraints are transformed. The cost function in (32) can be compactly denoted [33, 34] by

$$J_{(k)} = \vec{\mathbf{u}}_{(k)}^{T}\mathbf{H}_{(k)}\vec{\mathbf{u}}_{(k)} + 2\mathbf{x}_{0(k)}^{T}\mathbf{G}_{(k)}^{T}\vec{\mathbf{u}}_{(k)} + \mathbf{x}_{0(k)}^{T}\mathbf{F}_{(k)}\mathbf{x}_{0(k)}. \tag{46}$$

Since the part $\mathbf{x}_{0(k)}^{T}\mathbf{F}_{(k)}\mathbf{x}_{0(k)}$ does not depend on the optimization variable $\vec{\mathbf{u}}_{(k)}$ and contributes only a fixed value to the cost at each iteration, we may omit it from the optimization procedure. For the variable model structure, $\mathbf{H}_{(k)}$ and $\mathbf{G}_{(k)}$ are evaluated online at each step (k) by [33, 34]

$$\mathbf{H}_{(k)} = \sum_{i=0}^{n-1}\mathbf{N}_{i(k)}^{T}\mathbf{Q}\mathbf{N}_{i(k)} + \mathbf{N}_{n(k)}^{T}\mathbf{P}_{f(k)}\mathbf{N}_{n(k)} + \mathscr{R},$$
$$\mathbf{G}_{(k)} = \sum_{i=0}^{n-1}\mathbf{N}_{i(k)}^{T}\mathbf{Q}\mathbf{M}_{i(k)} + \mathbf{N}_{n(k)}^{T}\mathbf{P}_{f(k)}\mathbf{M}_{n(k)}, \tag{47}$$

where the index i denotes the ith block row, respectively, and n denotes the last block row of $\mathbf{N}_{(k)}$ and $\mathbf{M}_{(k)}$ identified, discretized, and computed for time (k). Matrix $\mathscr{R}$ is the block matrix with the input penalty $\mathbf{R}$ on its main diagonal. Using this formulation, the constraints defined by (43)–(45) are included in the cost function itself.

The upper and lower constraints in (41) which are enforced on all future input variables $\underline{u} \leq \vec{\mathbf{u}}_{(k)} < \overline{u}$ until the end of the horizon can be compactly expressed [34] by

$$\begin{bmatrix}\mathbf{I}\\ -\mathbf{I}\end{bmatrix}\vec{\mathbf{u}}_{(k)} \leq \begin{bmatrix}\mathbf{1}\overline{u}\\ -\mathbf{1}\underline{u}\end{bmatrix}. \tag{48}$$

In this case, the constraints define limits on the allowable voltage potential supplied to the actuators.

2.5. Adaptive-Predictive EKF-MPC Vibration Control Strategy. The resulting adaptive-predictive EKF-MPC control strategy can be summarized in the following algorithm [40].

Algorithm 1. Perform the following set of operations at each sampling instant (k):

(1) propagate the state $\hat{\mathbf{x}}_{a(k)}^{-}$ in (14) and covariance matrix $\dot{\mathbf{P}}(t)$ in (16) in simulation to obtain the a priori estimate;

(2) sample the actual deflection $y_{(k)}$ filtered by the low-pass and running mean filter;

(3) compute the Kalman gain $\mathbf{K}_{f(k)}$ using (19);

(4) based on the measurement sample and gain, update the state $\hat{\mathbf{x}}_{a(k)}^{+}$ through (20) to get a posteriori state estimates; then update the covariance matrix $\mathbf{P}_{(k)}^{+}$ in (21);

(5) based on the new parameters $\mathbf{p}_{(k)}$, reassemble the continuous system model $\mathbf{\Phi}_{(k)}$ and $\mathbf{\Gamma}_{(k)}$ by (4);

(6) approximate $\mathbf{\Psi}_{(k)}$ through (28) to discretize the system matrices $\mathbf{A}_{(k)}$ and $\mathbf{B}_{(k)}$ using (25);

(7) solve the discrete-time algebraic Riccati equation in (33) for the terminal weighting $\mathbf{P}_{f(k)}$ matrix using (34)–(38);

(8) use the discretized model to compute the state prediction matrices $\mathbf{M}_{(k)}$ and $\mathbf{N}_{(k)}$ by (30);

(9) use the state prediction matrices to compute the cost prediction matrices $\mathbf{H}_{(k)}$ and $\mathbf{G}_{(k)}$ through (46);

(10) minimize the quadratic MPC cost function $J_{(k)}$ in (46) subject to the following input constraints: $\overline{u} \leq u_{(k+i)} \leq \underline{u}$, $i = 0, 1, 2, \ldots, n-1$;

(11) apply the first element of the vector of optimal control moves $\vec{\mathbf{u}}_{(k)}$ to the controlled system;

(12) repeat the procedure from (1).

3. Laboratory Hardware and Experimental Settings

The experimental hardware (Figure 1(a)) consists of a cantilever beam fixed at one end and free at the other. Though it is very simple in its design, this lightly damped cantilever beam used here as the demonstration example may represent a wide variety of real-life structures [8, 38] from the standpoint of dynamic control, including wing surfaces [39], helicopter rotor blades [52], robotic manipulators in space [53], solar panels in space [54], and antenna systems [55].

The beam is made of commercially available pure aluminum in the dimensions of $550 \times 40 \times 3$ mm. The actuating elements are MIDÉ QP16n piezoelectric transducers made of PZT5A piezoceramic material (Figure 1(b)), housed in a film case with prefabricated electrical terminals. Actuators are connected counterphase to a MIDÉ EL-1225 amplifier and receive an analog control signal. The sensor is a Keyence LK-G82 laser triangulation system, connected to the Keyence LK-G3001V filtering and processing unit, providing an analog voltage signal to the controller (Figure 1(c)).

The external disturbance resembles transient vibration effects common in aerospace constructions [39] that are often introduced to cantilever-like structures using release tests [56–58]. Repeated impacts are delivered using the stinger mechanism, providing bursts of force at the free end of the beam using a linear motor controlled by a digital input signal (Figure 1(c)).

The EKF-MPC vibration control algorithm is developed in the MATLAB/Simulink environment, where all online algorithm stages are made compatible with the real-time capability of the software. Custom blocks such as the EKF algorithm, model reassembly, discretization, prediction, and others are developed in the MATLAB m-file scripting language and recompiled into C language for the Real-Time Workshop target using the Embedded MATLAB Editor.

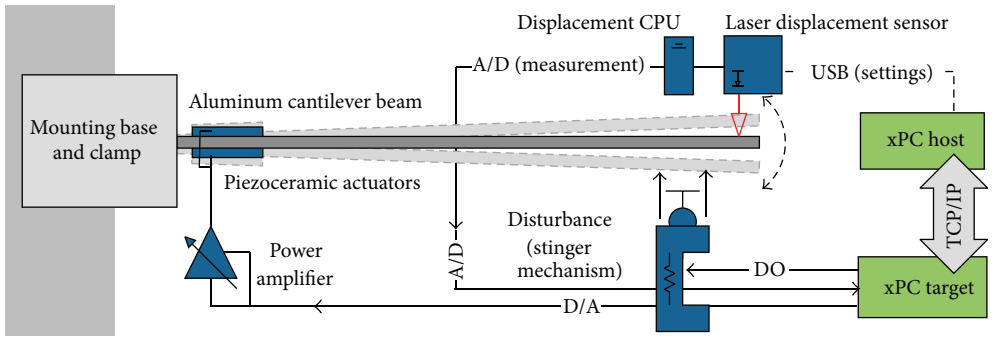

Figure 2: Schematic representation of the experimental system.

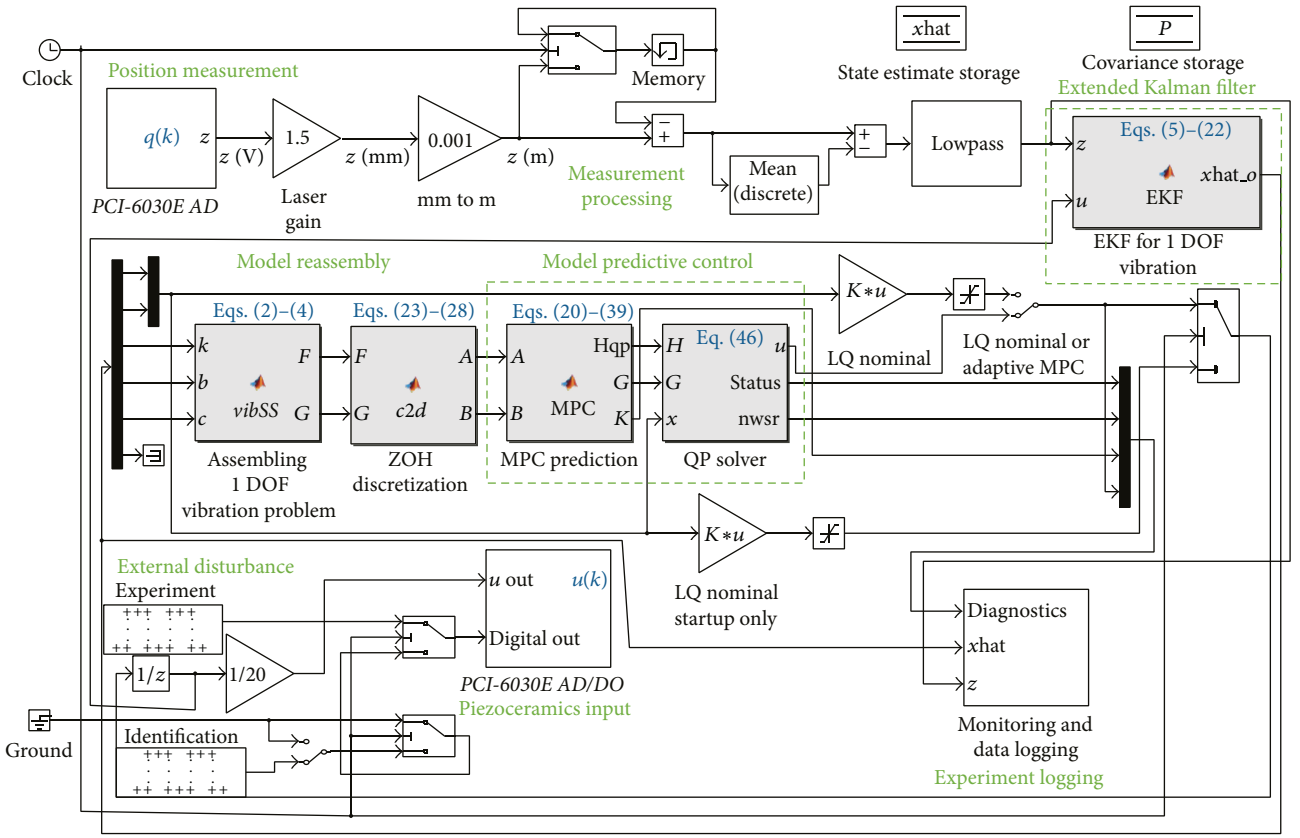

Figure 3: Simplified block scheme of the proposed adaptive vibration control algorithm.

The online Simulink block scheme of the controller algorithm is implemented on a personal computer running the MATLAB xPC Target rapid control software prototyping platform, connected to hardware components with a National Instruments PCI-6030E measurement card. The developed control system is loaded onto the Target platform via the TCP/IP protocol. The overall schematic representation of the experimental system is illustrated in Figure 2.

The simplified block scheme of the proposed adaptive vibration control algorithm is featured in Figure 3, where the essential blocks are emphasized. The position measurement is sampled in the block named *"PCI-6030E AD,"* and then it is scaled according to the linear amplification of the laser system and converted to meter units. The incoming signal is low- pass filtered and then the running mean is removed. This processed position measurement is used in the block named *"EKF"* to estimate the dynamic states and parameters of the system using (5)–(22). The estimated parameters are used to reassemble the continuous state-space model of the system in (2)–(4) by *"vibSS,"* and then the system matrices are discretized using the procedure in (23)–(28) in the block named *"c2d."* The prediction matrices are updated according to the new model in *"mpc"* based on (29)–(31), along with the current LQ gain and terminal weight based on (33)–(39). The cost function defined by (46) is minimized using quadratic programming in the block named *"QP Solver,"*

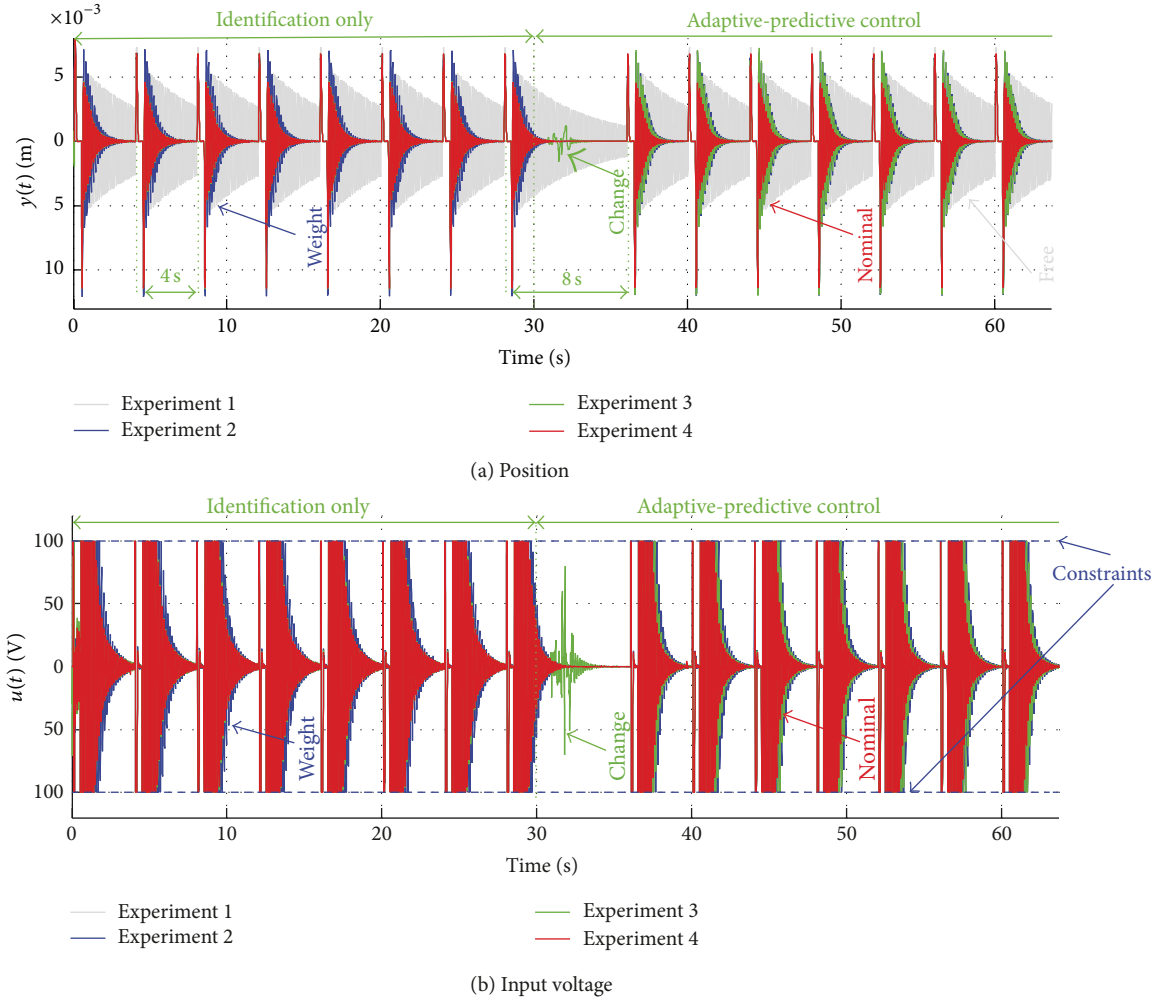

Figure 4: Experiment design: measured position output and actuator input.

which requires the Hessian, gradient, and a state estimate; the rest of the inputs such as the constraints are fixed. The first input is scaled down to the amplifier constant and sent to the output named *"PCI-6030E DA/DO."* The rest of the blocks are responsible for data logging and monitoring, timing and driving the stinger mechanism with the periodic disturbance signal fed to the digital output.

To evaluate the control strategy presented in Section 2, four experimental scenarios were considered. In all of these scenarios, during the first 30 s, the initial identification procedure was performed using the fixed LQ gain based on the initial parameter estimates and the settings of the MPC algorithm, excited by disturbance bursts spaced 4 s apart. This was followed by switching to the adaptive MPC control scheme and an 8 s pause; then, the disturbances spaced at 4 s apart continued. Figure 4 illustrates the experiment design with the different experimental settings. Experiment 1 (grey) assumed the original beam without added mass and the controllers switched off (open-loop control). The rest of the experiments used the EKF-MPC algorithm to generate the control inputs to the piezoceramic actuator. Experiment 2 (blue) assumed a small weight added to the end of the beam for the whole experiment, Experiment 3 (green) assumed that the weight was added manually during the pause after ~30 s, and finally Experiment 4 (red) assumed no added weight, just the original beam. The summary of experimental scenarios and settings is given in Table 1.

Table 1: Summary of experimental scenarios and settings.

Exp.	Control	Weight	Change t	Color
1	✗	✗	N/A	Grey
2	√	√	0 s	Blue
3	√	√	~30 s	Green
4	√	✗	N/A	Red

Global sampling times were set $T = 0.01$ s for all experiments, while the simulation step for the continuous part of the EKF algorithm was $dt = T/500 = 20\,\mu$s. The EKF was set with a fixed mass of $m = 0.178$ g, which is the real measured mass of the beam section starting from the clamp. An offline grey-box identification procedure [59] may result in a different weight parameter; however, it is important to realize that the dynamic weight may not correspond to the

physical weight and is highly dependent on the settings of the EKF.

For each experimental scenario, the initial augmented state estimate was

$$\hat{\mathbf{x}}_{a0}^{+} = \begin{bmatrix} 0 & 0 & 450 & 0.1 & 1E-3 & 0 \end{bmatrix}^{T}, \tag{49}$$

and the initial error covariance estimate matrix was set to

$$\mathbf{P}_{0}^{+} = \operatorname{diag}\begin{bmatrix} 1E-5 & 1E-2 & 1E+4 & 1E-2 & 1E-5 & 1E-1 \end{bmatrix}. \tag{50}$$

Measurement noise covariance for the single position output was $\mathbf{R}_f = R_f = 1E-9$, while the process noise covariance matrix was set to

$$\mathbf{Q}_{ft} = \operatorname{diag}\begin{bmatrix} 1E-10 & 1E-4 & 1E-2 & 1E-8 & 1E-12 & E-2 \end{bmatrix}. \tag{51}$$

Though the measurement noise covariance may seem to be too low, this is a physically meaningful setting; as the position varies in the range of millimeters and the precise optical measurement system implies only very slight inaccuracies. To prevent the estimation of negative parameters, an ad hoc clipping strategy [32, 40, 43] was used in the EKF.

The continuous model was discretized with an approximation of $\mathbf{\Psi}$ with $j = 10$ iterations. The MPC algorithm was set up using an input penalty $\mathbf{R} = R = 1E-10$, state penalty $\mathbf{Q} = \mathbf{C}^{T}\mathbf{C}$, input constraints $-100 \leq \vec{\mathbf{u}}_{(k)} < 100\,\mathrm{V}$ (see Figure 4(b)), no state constraints, and $n = 10$ steps prediction horizon. The constrained quadratic programming problem was solved online using the qpOASES active-set sequential quadratic programming solver [60–62], which is specifically designed for solving optimization problems occurring in MPC. The measurement chain included a low-pass FIR filter with the passband edge at 30 Hz and stopband edge at 50 Hz and a windowed running mean filter with a 0.1 Hz fundamental frequency.

4. Results and Discussion

Figure 5 shows a detailed view of the measured position $x_{1(k)} = q(k)$ (Figure 5(a)), estimated velocity $x_{2(k)} = \dot{q}(k)$ (Figure 5(b)), input voltage $u_{(k)}$ (Figure 5(c)), and disturbance force $F_{e(k)}$ (Figure 5(d)) for a selected time window of 15 s. The initial identification procedure ends at the 30 s, just after the second disturbance, and the adaptive EKF-MPC algorithm continues to take over the control of the beam.

From the measured positions shown in Figure 5(a), it is clear that in all experiments with the EKF-MPC (Experiments 2–4) the vibration levels are attenuated very effectively; in fact, settling times are shorter by approximately a factor of ten when compared to the open-loop case (Experiment1). The settling time for closed-loop control is approximately $t_s \cong 1.9\,\mathrm{s}$, while the open-loop system does not settle until the next impact is delivered from the stinger ($t_s \gg 4\,\mathrm{s}$, where t_s is 5% of the position of the largest amplitude at impact). The difference between the considered experimental scenarios is more subtle but still visible on both Figures 5(a) and 5(b), where the lightest beam with the nominal weight produces the smallest vibration amplitudes and speeds (Experiment 4), while the perturbed physical parameters caused by a weight (Experiments 2, 3) result in slightly larger vibration amplitudes and speeds.

In spite of the added weight and increased deformation amplitudes, the EKF-MPC algorithm compensates for the change in the dynamics by using more agile inputs, which is demonstrated in the longer lasting evolution of input voltages having greater amplitudes outside the constrained region. Note the intensity of the inputs in Figure 5(c), where this effect is especially evident in the case of Experiment 3 (before and after the mass has been added) and the difference between the input behavior in the case of Experiment 2 versus Experiment 4. The larger mass in Experiment 2 results in more aggressive inputs than in Experiment 4, while the effects of the mass increase in Experiment 3 are demonstrated after a short adaptation period.

These results suggest that the proposed EKF-MPC algorithm enables the system to maintain the time required to settle comparable in all closed-loop control cases (Experiments 2–4). These matching settling times are a consequence of increased input activity on the piezoceramic elements. In addition to the adaptation feature, the constrained infinite horizon model predictive algorithm respects the process constraints imposed on the inputs throughout the experiments (Figure 5(c)). Figure 5(d) shows the estimated force disturbance. The shock-like disturbance force $F_{e(k)}$ is somewhat distorted by the low-pass and running mean filtering on the measured inputs; however, as one would expect, it remains consistent throughout all experimental scenarios (Experiments 1 and 4).

Figure 6 shows the estimated parameters and the equivalent LQ gain for the whole duration of the experiments. The estimated spring constant $k_{(k)}$ is shown in Figure 6(a), damping constant $b_{(k)}$ in Figure 6(b), and the force conversion constant $c_{(k)}$ in Figure 6(c). The unconstrained equivalent LQ gain is shown for diagnostic purposes only in Figure 6(d) in order to illustrate the adaptive behavior of the EKF-MPC control algorithm.

All the parameters simultaneously demonstrate a change to actively compensate for the mass added to the system, since the mass itself is not an extra identified but a fixed parameter. The dynamic model used in the MPC algorithm represents an equivalent point-mass-damper system instead of the real cantilever beam; therefore, the variations in the mass translate to a hypothetical change in other equivalent model parameters. These are to be understood merely as analogous changes in stiffness, damping, or actuator efficiency.

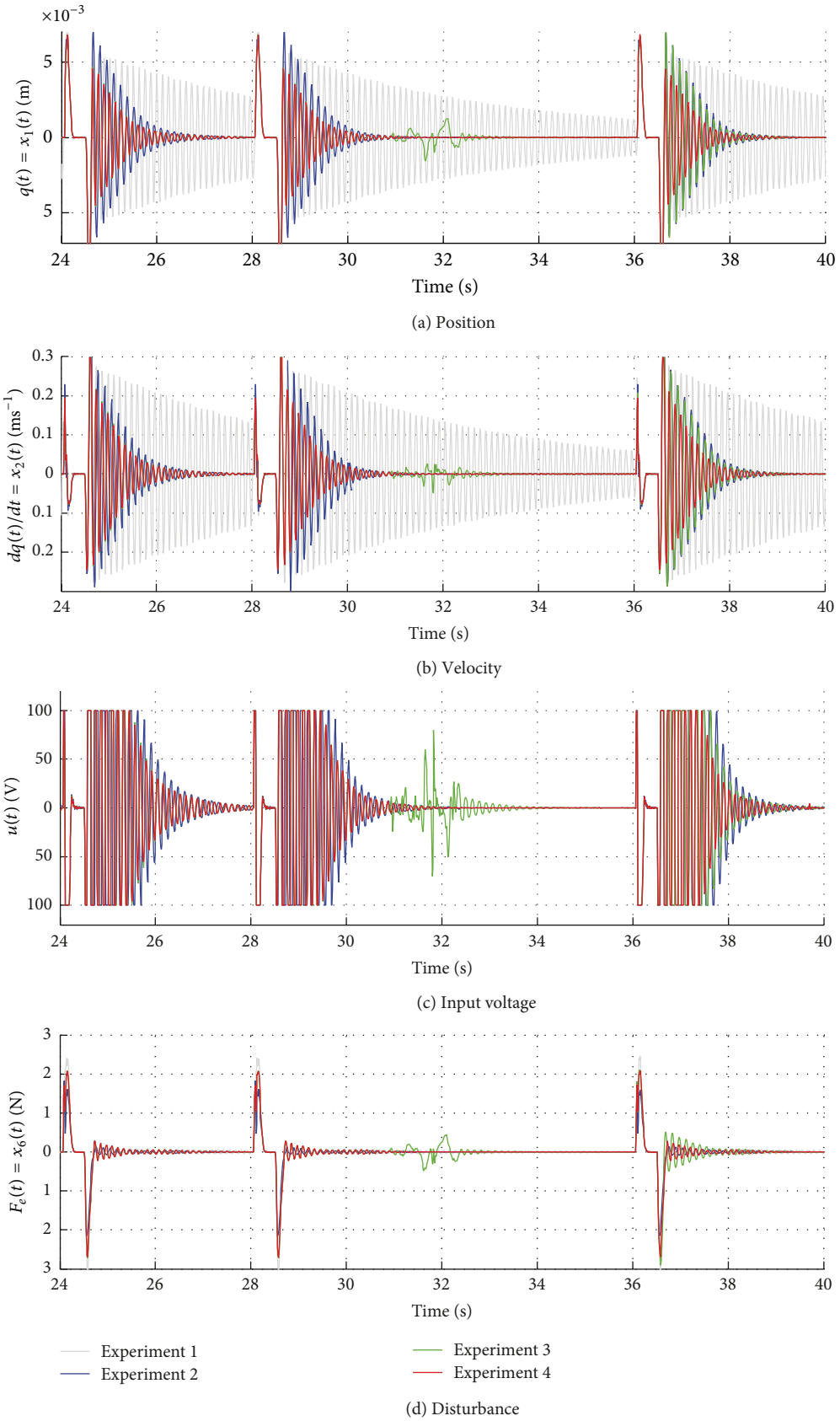

Figure 5: Detail of the estimated system states, control input, and disturbance force.

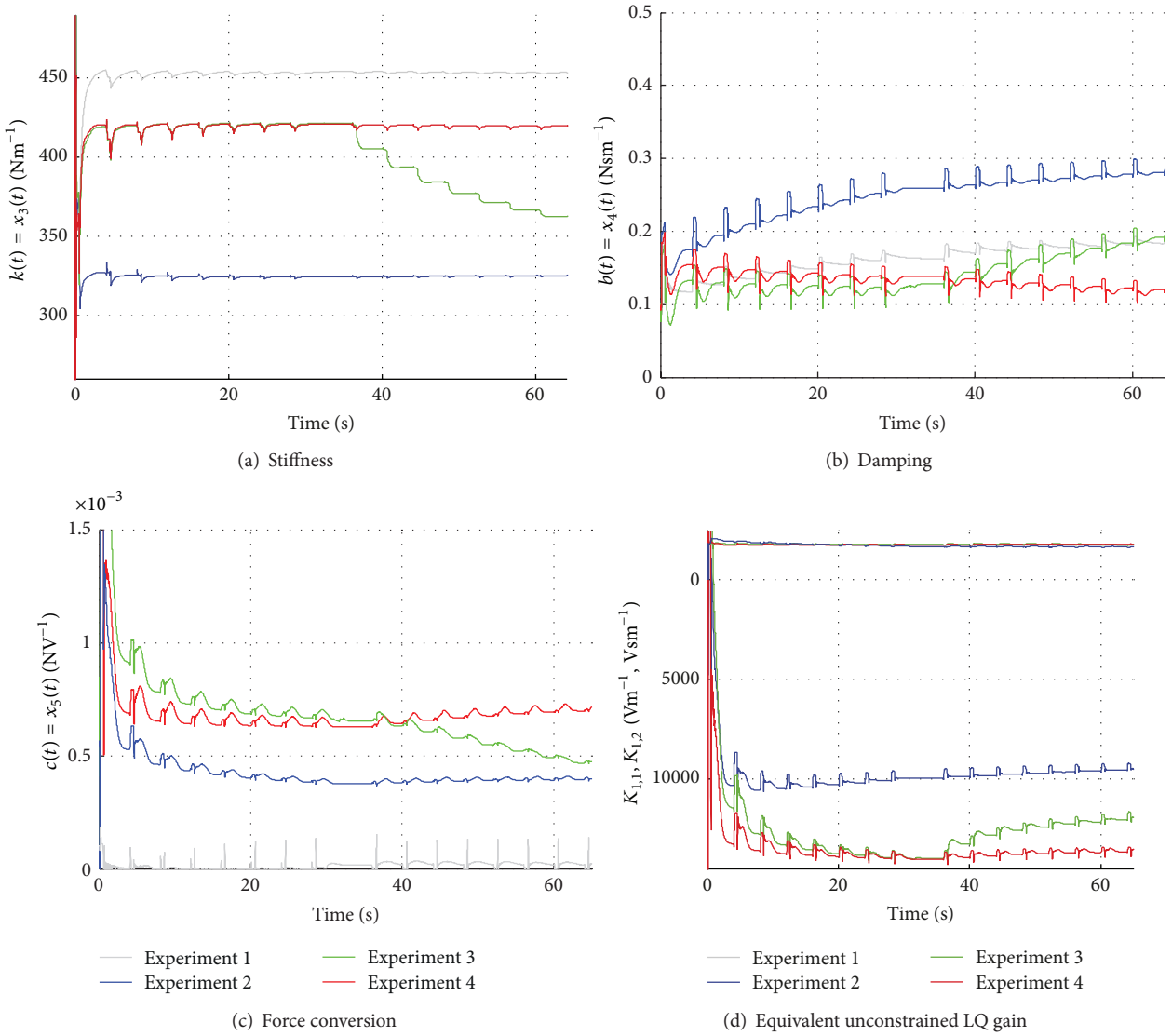

FIGURE 6: Estimated model parameters and the equivalent unconstrained LQ gain.

Overall, the equivalent stiffness, force conversion constant, and the $\mathbf{K}_{1,1}$ component of the LQ gain drop with increased mass, while damping increases. The sudden spikes visible in all parameters are due to the mismatch between the impulse-like disturbance of the stinger mechanism and the formulation of the EKF algorithm, which is expecting only centered Gaussian noise as disturbance [24–26]. Of the three identified parameters, stiffness was the most stable and consistent one, while the online identification of the damping parameter proved to be somewhat challenging.

In case the mass is kept constant during the entire duration of the test (Experiments 1, 2, and 4), all the parameters adapt to the changes in the system dynamics during the initial identification phase and then are kept on these levels even after the EKF-MPC algorithm takes over. When the mass is added to the beam just before 40 s (Experiment 3), the adaptation process starts only after this time. The parameter variations are translated as the model updates in the MPC algorithm.

In practical applications, especially with joint state and parameter estimation, the excitation of the dynamic system may be absent at certain operation times. The proposed method works well with information-rich processes, however, it has not been tested with nonpersistent excitation signals. The EKF is known to degrade in performance or even become unstable in the absence of excitation as a result of ill-conditioned numerical operations [63].

5. Conclusions

An adaptive active vibration control algorithm based on the extended Kalman filter for real-time parameter estimation and the infinite horizon dual-mode constrained model predictive algorithm has been proposed for fixed-free cantilevers in this paper. The EKF-MPC algorithm has been implemented and experimentally tested in real time on the laboratory system featuring an aluminum beam with piezoceramic actuation and position feedback.

Four experimental scenarios were used to evaluate the proposed EKF-MPC adaptive control algorithm. The closed-loop settling times were reduced by a factor of ten in all cases, while the controller promptly reacted to changes in the beam dynamics. The mass increase, emulated by the added weight, induced change in the estimated parameters of the equivalent point-mass-damper system. This mass increase resulted in the harder-to-control system requiring increased control inputs. In fact, according to the experimental results presented here, the parameter changes translated to the MPC algorithm resulted in more aggressive control moves.

The proposed EKF-MPC algorithm unifies the key features of both methods, introducing adaptivity and constraint handling to the vibration control of flexible cantilever beam-like structures.

5.1. Future Work. Certain aspects of the unmodeled dynamics, namely, the effect of the outside disturbance, may cause the identification algorithm to diverge (not shown in the experiments here). These drawbacks will be addressed in an upcoming work [64] by the introduction of spectrum shaping filters [25, 26] into the augmented models and possibly by selective error covariance matrix update disabling during disturbances.

The performance and stability of the proposed algorithm have not been tested in operation modes without significant outside excitation. The nonpersistent excitation may result in an ill-posed numerical problem and stability problems in the online EKF component. A possible solution to this problem may be the use of the moving horizon observer instead of the EKF, as it is suggested here. Instead of producing estimates based on the last know measurement and a recursive procedure, the MHO uses a moving window of past measurements. While this alone may increase the efficiency of the estimation procedure faced with nonpersistent data, the MHO variants enhanced by regularization mechanisms to cope with this situation have been suggested [63]. The price of eliminating these problems using the MHO is a heavy increase in computation cost, as the MHO requires the use of online nonlinear constrained optimization procedures. The use of MHO to estimate the states and parameters of vibration dynamics has been demonstrated in simulation [32] and using offline measurement data for a nanopositioner mechanism [65]. Real-time use of the MHO for vibration mechanics and adaptive vibration control is currently under development, but an online experimental implementation of the estimator alone has been recently proposed [66].

Another relevant matter requiring attention in upcoming research is the question of the stability of the MPC component of the proposed algorithm. Stability guarantees may be given for linear systems and nominal models by enforcing recursive constraints beyond the control horizon [46, 47]; however, the stability issue of MPC in face of uncertainties—also known as stochastic MPC—is a more complex issue [67]. Recent advancements in the field of uncertain and robust MPC formulations can address this problem effectively [68–70].

An important aspect of self-reliance in an adaptive structural control scheme is process monitoring and fault diagnostics; thus, in addition to the adaptive features discussed in this paper, online system diagnostics can be also easily included in the formulation, since adaptive control requires some form of online system identification. In addition to the advanced model-based fault diagnostics methods [23, 71], recent advances in data-driven fault tolerant control [72–74] can be an attractive way to increase the self-reliance of active vibration control.

Conflict of Interests

The authors declare that there is no conflict of interests regarding the publication of this paper.

Acknowledgments

The authors would like to gratefully acknowledge the financial support granted by the Slovak Research and Development Agency (APVV) under Contracts APVV-0090-10, APVV-0131-10, and APVV 0280-06 and by the Scientific Grant Agency (VEGA) of the Ministry of Education, Science, Research and Sport of the Slovak Republic under Contract 1/0138/11. The authors wish to thank J. Csambál for his design and implementation work on the stinger mechanism and its electronic drive stage used in the paper. The authors would also like to thank T. A. Johansen for his advice offered during the preparation of this work.

References

[1] A. Montazeri, J. Poshtan, and A. Choobdar, "Performance and robust stability trade-off in minimax LQG control of vibrations in flexible structures," *Engineering Structures*, vol. 31, no. 10, pp. 2407–2413, 2009.

[2] A. Preumont, *Vibration Control of Active Structures*, Kluwer Academic, 2nd edition, 2002.

[3] C. R. Fuller, S. J. Elliott, and P. A. Nelson, *Active Control of Vibration*, Academic Press, San Francisco, Calif, USA, 1st edition, 1996.

[4] H. Benaroya and M. L. Nagurka, *Mechanical Vibration: Analysis, Uncertainities and Control*, CRC Press/Taylor & Francis, Boca Raton, Fla, USA, 3rd edition, 2010.

[5] N. Chandiramani and S. Purohit, "Semi-active control using magnetorhelogical dampers with output feedback and distributed sensing," *Shock and Vibration*, vol. 19, no. 6, pp. 1427–1443, 2012.

[6] A. Wills, D. Bates, A. Fleming, B. Ninness, and R. Moheimani, "Application of MPC to an active structure using sampling rates up to 25 kHz," in *Proceedings of the 44th IEEE Conference on Decision and Control, and the European Control Conference (CDC-ECC '05)*, pp. 3176–3181, December 2005.

[7] M. Hassan, R. Dubay, C. Li, and R. Wang, "Active vibration control of a flexible one-link manipulator using a multivariable predictive controller," *Mechatronics*, vol. 17, no. 1, pp. 311–323, 2007.

[8] G. Takács and B. Rohal'-Ilkiv, *Predictive Vibration Control: Efficient Constrained MPC Vi-Bration Control for Lightly Damped Mechanical Systems*, Springer, London, UK, 2012.

[9] D. C. Hyland and L. D. Davis, "Toward self-reliant control for adaptive structures," *Acta Astronautica*, vol. 51, no. 1–9, pp. 89–99, 2002.

[10] X. Yalan, C. Jianjun, and W. Xiaobing, "Robust vibration control of uncertain flexible structures with poles placement," in *Proceedings of the 1st International Symposium on Systems and Control in Aerospace and Astronautics (ISSCAA '06)*, pp. 350–354, January 2006.

[11] W.-H. Jee and C.-W. Lee, "H∞ robust control of flexible manipulator vibration by using a piezoelectric-type servo-damper," *Control Engineering Practice*, vol. 2, no. 3, pp. 421–430, 1994.

[12] Y.-R. Hu and A. Ng, "Active robust vibration control of flexible structures," *Journal of Sound and Vibration*, vol. 288, no. 1-2, pp. 43–56, 2005.

[13] J. Fei, "Adaptive vibration control schemes for flexible structure," in *Proceedings of the IEEE International Conference on Mechatronics and Automation (ICMA '07)*, pp. 2547–2552, August 2007.

[14] S. J. Elliott and P. A. Nelson, "Active noise control," *IEEE Signal Processing Magazine*, vol. 8, no. 10, pp. 12–35, 1993.

[15] Z. Zhang, F. Hu, Z. Li, and H. Hua, "Modeling and control of the vibration of two beams coupled with fluid and active links," *Shock and Vibration*, vol. 19, no. 4, pp. 653–668, 2012.

[16] S. Griffin, A. Weston, and J. Anderson, "Adaptive noise cancellation system for low frequency transmission of sound in open fan aircraft," *Shock and Vibration*, vol. 20, no. 5, pp. 989–1000, 2013.

[17] T. Nestorović Trajkov, H. Köppe, and U. Gabbert, "Direct Model Reference Adaptive Control (MRAC) design and simulation for the vibration suppression of piezoelectric smart structures," *Communications in Nonlinear Science and Numerical Simulation*, vol. 13, no. 9, pp. 1896–1909, 2008.

[18] M.-C. Pai, "Closed-loop input shaping control of vibration in flexible structures via adaptive sliding mode control," *Shock and Vibration*, vol. 19, no. 2, pp. 221–233, 2012.

[19] M. Xin and J. Fei, "Adaptive vibration control for MEMS vibratory gyroscope using backstepping sliding mode control," *Journal of Vibration and Control*, 2013.

[20] S.-H. Youn, J.-H. Han, and I. Lee, "Neuro-adaptive vibration control of composite beams subject to sudden delamination," *Journal of Sound and Vibration*, vol. 238, no. 2, pp. 215–231, 2000.

[21] R. Kumar, S. P. Singh, and H. N. Chandrawat, "MIMO adaptive vibration control of smart structures with quickly varying parameters: neural networks vs classical control approach," *Journal of Sound and Vibration*, vol. 307, no. 3–5, pp. 639–661, 2007.

[22] W. Zhang, G. Meng, and H. Li, "Adaptive vibration control of micro-cantilever beam with piezoelectric actuator in MEMS," *The International Journal of Advanced Manufacturing Technology*, vol. 28, no. 3-4, pp. 321–327, 2006.

[23] M. Zghal, L. Mevel, and P. D. Moral, "Modal parameter estimation using interacting Kalman filter," *Mechanical Systems and Signal Processing*, 2012.

[24] A. Gelb, *Applied Optimal Estimation*, The MIT Press, Cambridge, Mass, USA, 1974.

[25] D. Simon, *Optimal State Estimation: Kalman, H∞, and Nonlinear Approaches*, Wiley-Interscience, New York, NY, USA, 1st edition, 2006.

[26] P. S. Maybeck, *Stochastic Models, Estimation and Control*, vol. 141 of *Mathematics in Science and Engineering*, Academic Press, New York, NY, USA, 1st edition, 1979.

[27] E. Lourens, E. Reynders, G. De Roeck, G. Degrande, and G. Lombaert, "An augmented Kalman filter for force identification in structural dynamics," *Mechanical Systems and Signal Processing*, vol. 27, no. 1, pp. 446–460, 2012.

[28] T. Mu, L. Zhou, and J. Yang, "Adaptive extended Kalman filter for parameter tracking of baseisolated structure under unknown seismic input," in *Proceedings of the 10th International Bhurban Conference on Applied Sciences and Technology (IBCAST '13)*, pp. 84–88, 2013.

[29] A. Turnip, K. S. Hong, and S. Park, "Modeling of a hydraulic engine mount for active pneumatic engine vibration control using the extended Kalman filter," *Journal of Mechanical Science and Technology*, vol. 23, no. 1, pp. 229–236, 2009.

[30] K. Szabat and T. Orlowska-Kowalska, "Adaptive control of two-mass system using nonlinear extended Kalman Filter," in *Proceedings of the 32nd IEEE Annual Conference on Industrial Electronics (IECON '06)*, pp. 1539–1544, November 2006.

[31] K. Szabat and T. Orlowska-Kowalska, "Application of the extended Kalman filter in advanced control structure of a drive system with elastic joint," in *Proceedings of the IEEE International Conference on Industrial Technology (IEEE ICIT '08)*, pp. 1–6, April 2008.

[32] T. Polóni, B. Rohal'-Ilkiv, and T. A. Johansen, "Damped one-mode vibration model state and parameter estimation via prefiltered moving horizon observer," in *Proceedings of the 5th IFAC Symposium on Mechatronic Systems (Mechatronics '10)*, pp. 24–31, Boston, Mass, USA, September 2010.

[33] J. A. Rossiter, *Model-Based Predictive Control: A Practical Approach*, CRC Press, Boca Raton, Fla, USA, 1st edition, 2003.

[34] J. M. Maciejowski, *Predictive Control With Constraints*, Prentice Hall, Upper Saddle River, NJ, USA, 2000.

[35] J. H. Lee, "Model predictive control: review of the three decades of development," *International Journal of Control, Automation and Systems*, vol. 9, no. 3, pp. 415–424, 2011.

[36] E. N. Pistikopoulos, "From multi-parametric programming theory to MPC-on-a-chip multiscale systems applications," *Computers & Chemical Engineering*, vol. 47, pp. 57–66, 2012.

[37] G. Takács and B. Rohal'-Ilkiv, "Model predictive control algorithms for active vibration control: a study on timing, performance and implementation properties," *Journal of Vibration and Control*, 2013.

[38] R. Y. Chiang and M. G. Safonov, "Design of H∞ controller for a lightly damped system using a bilinear pole shifting transform," in *Proceedings of the American Control Conference*, pp. 1927–1928, June 1991.

[39] J. Richelot, J. B. Guibe, and V. P. Budinger, "Active control of a clamped beam equipped with piezoelectric actuator and sensor using generalized predictive control," in *Proceedings of the IEEE International Symposium on Industrial Electronics (IEEE-ISlE '04)*, vol. 1, pp. 583–588, May 2004.

[40] G. Takács, T. Polóni, and B. Rohal'-Ilkiv, "Adaptive model predictive vibration control with state and parameter estimation using extended Kalman filtering," in *Proceedings of the 20th International Congress on Sound and Vibration (ICSV '13)*, pp. 611/1–611/8, Bangkok, Thailand, July 2013.

[41] N. P. Jones, T. Shi, J. Hugh Ellis, and R. H. Scanlan, "System-identification procedure for system and input parameters in ambient vibration surveys," *Journal of Wind Engineering and Industrial Aerodynamics*, vol. 54-55, pp. 91–99, 1995.

[42] V. Namdeo and C. S. Manohar, "Nonlinear structural dynamical system identification using adaptive particle filters," *Journal of Sound and Vibration*, vol. 306, no. 3–5, pp. 524–563, 2007.

[43] T. Polóni, A. A. Eielsen, B. Rohal'-Ilkiv, and T. Johansen, "Moving horizon observer for vibration dynamics with plant uncertainties in nanopositioning system estimation," in *Proceedings*

of the American Control Conference (ACC '12), pp. 3817–3824, 2012.

[44] G. F. Franklin, J. D. Powell, and M. L. Workman, *Digital Control of Dynamic Systems*, Addison-Wesley, Boston, Mass, USA, 3rd edition, 1997.

[45] P. O. M. Scokaert and J. B. Rawlings, "Infinite horizon linear quadratic control with constraints," in *Proceedings of the World Congress (IFAC '96)*, vol. 7, pp. 109–114, San Francisco, Calif, USA, 1996.

[46] H. Chen and F. Allgöwer, "A quasi-infinite horizon nonlinear model predictive control scheme with guaranteed stability," *Automatica*, vol. 34, no. 10, pp. 1205–1217, 1998.

[47] D. Q. Mayne, J. B. Rawlings, C. V. Rao, and P. O. M. Scokaert, "Constrained model predictive control: stability and optimality," *Automatica*, vol. 36, no. 6, pp. 789–814, 2000.

[48] T. Pappas, A. J. Laub, and N. R. Sandell Jr., "On the numerical solution of the discrete-time algebraic Riccati equation," *IEEE Transactions on Automatic Control*, vol. 25, no. 4, pp. 631–641, 1980.

[49] M. Corless, *Linear Systems and Control: A First Course*, Course notes for AAE 564, Purdue University, West Lafayette, Ind, USA, 2008.

[50] A. J. Laub, "A Schur method for solving algebraic Riccati equations," *IEEE Transactions on Automatic Control*, vol. 24, no. 6, pp. 913–921, 1979.

[51] W. F. Arnold III and A. J. Laub, "Generalized eigenproblem algorithms and software for algebraic Riccati equations," *Proceedings of the IEEE*, vol. 72, no. 12, pp. 1746–1754, 1984.

[52] H. Lu and G. Meng, "An experimental and analytical investigation of the dynamic characteristics of a flexible sandwich plate filled with electrorheological fluid," *International Journal of Advanced Manufacturing Technology*, vol. 28, no. 11-12, pp. 1049–1055, 2006.

[53] M. Sabatini, P. Gasbarri, R. Monti, and G. B. Palmerini, "Vibration control of a flexible space manipulator during on orbit operations," *Acta Astronautica*, vol. 73, pp. 109–121, 2012.

[54] Q. Hu, "A composite control scheme for attitude maneuvering and elastic mode stabilization of flexible spacecraft with measurable output feedback," *Aerospace Science and Technology*, vol. 13, no. 2-3, pp. 81–91, 2009.

[55] B. N. Agrawal and H. Bang, "Adaptive structures for large precision antennas," *Acta Astronautica*, vol. 38, no. 3, pp. 175–183, 1996.

[56] C. M. A. Vasques and J. Dias Rodrigues, "Active vibration control of smart piezoelectric beams: comparison of classical and optimal feedback control strategies," *Computers and Structures*, vol. 84, no. 22-23, pp. 1402–1414, 2006.

[57] S. B. Choi, Y. K. Park, and T. Fukuda, "A proof-of-concept investigation on active vibration control of hybrid smart structures," *Mechatronics*, vol. 8, no. 6, pp. 673–689, 1998.

[58] A. Grewal and V. J. Modi, "Robust attitude and vibration control of the space station," *Acta Astronautica*, vol. 38, no. 3, pp. 139–160, 1996.

[59] L. Ljung, *System Identification: Theory for the User*, PTR Prentice Hall, Upper Saddle River, NJ, USA, 2nd edition, 1999.

[60] H. J. Ferreau, H. G. Bock, and M. Diehl, "An online active set strategy to overcome the limitations of explicit MPC," *International Journal of Robust and Nonlinear Control*, vol. 18, no. 8, pp. 816–830, 2008.

[61] H. J. Ferreau, *An online active set strategy for fast solution of parametric quadratic programs with applications to predictive engine control [M.S. thesis]*, University of Heidelberg, 2006.

[62] H. J. Ferreau, "qpOASES—Online Active Set Strategy," 2013, http://www.qpoases.org.

[63] D. Sui and T. A. Johansen, "Moving horizon observer with regularisation for detectable systems without persistence of excitation," *International Journal of Control*, vol. 84, no. 6, pp. 1041–1054, 2011.

[64] G. Takács, T. Polóni, and B. Rohal'-Ilkiv, "Adaptive predictive control of transient vibrations in cantilevers with changing weight," in *Proceedings of the 19th World Congress of the International Federation of Automatic Control (IFAC '14)*, pp. 396/1–396/9, Cape Town, South Africa, August 2014.

[65] T. Polóni, A. A. Eielsen, B. Rohal'-Ilkiv, and T. A. Johansen, "Adaptive model estimation of vibration motion for a nanopositioner with moving horizon optimized extended Kalman filter," *Journal of Dynamic Systems, Measurement, and Control*, vol. 135, no. 4, Article ID 041019, 2013.

[66] G. Takács, T. Polóni, and B. Rohal'-Ilkiv, "Pseudo real-time state and parameter estimation of a vibrating active cantilever using the moving horizon observer," in *Proceedings of the 21th International Congress on Sound and Vibration (ICSV '14)*, pp. 820/1–820/8, Beijing, China, July 2014.

[67] D. Mayne, "Model predictive control: the challenge of uncertainty," in *Proceedings of the IEE Two-Day Workshop on Model Predictive Control: Techniques and Applications*, pp. 6/1–6/5, 1999.

[68] M. Cannon, B. Kouvaritakis, and D. Ng, "Probabilistic tubes in linear stochastic model predictive control," *Systems and Control Letters*, vol. 58, no. 10-11, pp. 747–753, 2009.

[69] M. Cannon, Q. Cheng, B. Kouvaritakis, and S. V. Raković, "Stochastic tube MPC with state estimation," *Automatica*, vol. 48, no. 3, pp. 536–541, 2012.

[70] J. Buerger, M. Cannon, and B. Kouvaritakis, "An active set solver for input-constrained robust receding horizon control," *Automatica*, vol. 50, no. 1, pp. 155–161, 2014.

[71] G. Takács and B. Rohal'-Ilkiv, "Real-time diagnostics of mechanical failure for thin active cantilever beams using low-cost hardware," in *Proceedings of the 7th Forum Acusticum Joined with the 61st Open Seminar on Acoustics*, Cracow, Poland, September 2014.

[72] S. Yin, S. X. Ding, A. Haghani, H. Hao, and P. Zhang, "A comparison study of basic datadriven fault diagnosis and process monitoring methods on the benchmark Tennessee Eastman process," *Journal of Process Control*, vol. 22, no. 9, pp. 1567–1581, 2012.

[73] S. Yin, S. X. Ding, A. H. Abandan Sari, and H. Hao, "Data-driven monitoring for stochastic systems and its application on batch process," *International Journal of Systems Science*, vol. 44, no. 7, pp. 1366–1376, 2013.

[74] S. Yin, H. Luo, and S. Ding, "Real-time implementation of fault-tolerant control systems with performance optimization," *IEEE Transactions on Industrial Electronics*, vol. 61, no. 5, pp. 2402–2411, 2014.